Modified Vitiation in a Moderate or Intense Low-Oxygen Dilution (MILD) Combustion Furnace

ARTICLE *in* ENERGY & FUELS · OCTOBER 2011

Impact Factor: 2.79 · DOI: 10.1021/ef201161x

energy&fuels

ARTICLE

pubs.acs.org/EF

Modified Vitiation in a Moderate or Intense Low-Oxygen Dilution (MILD) Combustion Furnace

J. Mi,*,† F. Wang,† P. Li,† and B. B. Dally‡

†State Key Laboratory of Turbulence and Complex Systems and Department of Energy and Resources Engineering, College of Engineering, Peking University, Beijing 100871, People's Republic of China

‡School of Mechanical Engineering, The University of Adelaide, Adelaide, South Australia 5005, Australia

ABSTRACT: This paper reports on the effects of various operational and geometric parameters on mixing and vitiation in a laboratory-scale furnace operating with natural gas and under the moderate or intense low-oxygen dilution (MILD) regime. The study is carried out through numerical modeling. Seven independent parameters are considered: i.e., mass fraction (f) of fuel diluents (CO_2 and N_2), air preheat temperature (T_a), global equivalence ratio (ϕ), air nozzle exit diameter (D_a), fuel nozzle exit diameter (D_f), fuel−air nozzles separation distance (S), and fuel injection angle from the furnace floor (α). The modeling is initially verified through a comparison to measurements by Szegö et al. (Szegö, G. G.; Dally, B. B.; Nathan, G. J. *Combust. Flame* **2008**, *154*, 281−295) in the same furnace geometry. It is shown that varying each of the parameters f, ϕ, D_a, D_f, S, and α can considerably influence the fuel-jet penetration distance and the recirculation rate of the exhaust gas, two important quantities for establishing the MILD combustion. Relatively, the geometric parameters D_a, D_f, S and α play more effective roles in controlling the vitiation rate and, hence, "flame" characteristics. Also, it is revealed that influences of all of the parameters, except S and α, can be represented by that of the ratio of the fuel injection momentum to the air injection momentum.

1. INTRODUCTION

Conservation of energy requires an efficient combustion of fossil fuels, while the protection of the environment demands a limitation of the pollutants emitted from combustion systems. A well-known method to improve combustion efficiency is to use the exhaust gas to preheat the combustion air by means of a heat exchanger. However, preheating the combustion air generally increases the flame temperature and, thus, the formation of thermal nitrogen oxides (NO_x). In this sense, the moderate or intense low-oxygen dilution (MILD) combustion,[1] also termed high-temperature air combustion (HiTAC)[2] or flameless oxidation (FLOX),[3] is hence qualified as one of the most successful combustion technologies developed in the last 2 decades or so. This combustion can be implemented using highly preheated air (around 1000 °C) externally by hot exhaust gas and/or internally by proper mixing of the fuel, air, and flue gas recirculated, so that reactants are intensely diluted and rapidly heated before reaction.[2] This process is also referred to as vitiation. Reactions under these conditions occur in a distributed reaction zone with a reduced peak temperature, and no visible flame is observed, hence, the term "flameless". As a consequence, the temperature is nearly uniform, the net radiation flux may be increased by as much as 30%, and pollutant emissions, especially NO_x, are much lower than that from conventional stabilized flames.[2]

Following the above findings, the MILD combustion itself and its technologies for industrial applications have been selected as significant subjects of research and development.[3−21] The gas fuel MILD burners have been implemented quite successfully in steel, ceramic, and glass furnaces.[4,5] However, their operating range has been found to be quite narrow,[2] and their performance largely depends upon heat recovery systems for air preheat.[6] More generally, such furnace systems are currently limited to a fairly small range of working conditions of various applications because of the absence of basic knowledge in the field.[1] To address this issue, more fundamental studies are needed on the related physical and chemical processes that determine critical parameters for successful operation of the MILD furnaces. The stabilization of MILD combustion, for example, is particularly an important issue. Contrary to conventional flame systems, which are commonly fitted with flame holders to avoid liftoff and blowout, MILD burners have to "extinguish" traditional visible flames near the burner exit. This extinguishing can be accomplished by either postponing the start location of the molecular mixing between non-premixed reactants (diffusion case) or elevating the injection speed of premixed reactants. Essentially, the MILD combustion requires local temperatures above the autoignition point and low oxygen concentrations, typically <10%, for stable operation. The mechanism to satisfy these conditions and to control the oxidation process mainly relies on the effective mixing process of fuel and oxygen. It is therefore necessary to explore the correlation of MILD combustion with its operational conditions, such as burner geometric parameters and fuel−air injection conditions.

Weber et al.[7,8] performed a series of experiments on the MILD combustion of gaseous, liquid, and solid fuels. Their measurements were conducted inside a furnace operating with a highly preheated air regime (1300 °C). Their data for natural gas (NG)

Special Issue: 2011 Sino-Australian Symposium on Advanced Coal and Biomass Utilisation Technologies

Received: August 2, 2011
Revised: October 4, 2011
Published: October 06, 2011

showed that a substantial improvement in the net flux of thermal radiation can be achieved under the MILD combustion. Both the mixing pattern and intensity have significant effects on the overall performance of the furnace firing with NG, specifically on the thermal efficiency part. The combustion process of light oil is very similar to that of NG, with invisible flames. However, combustion of heavy fuel oil and coal is significantly different, and the flames are always visible in their tests. Weber et al.[8] pointed out that further research is still needed to optimize the gas burner designs for maximizing the recirculation and mixing inside the furnace. Note that their test furnace of the square cross-section is characterized by a burner with a central (vitiated) air nozzle and two small off-axis fuel injectors and an exhaust outlet opposite the burner inlets (forward-flow furnace). Studies of the MILD combustion using a similar burner−furnace configuration have also been performed experimentally by, e.g., Rottier et al.[9] and numerically by the present authors.[10]

Szegö et al.[11,12] investigated operational characteristics of a parallel MILD combustion burner system in a furnace of different configurations. In their setup (backward-flow furnace), fuel is injected through four off-axis holes and air enters through a central nozzle, while four exhaust ports are located in between (see Figure 1). These investigators reported measurements of the temperature and exhaust gas composition from conventional and MILD combustions using NG and liquefied petroleum gas (LPG) as fuels. Their investigation[11,12] and that of Dally et al.[13] found that fuel dilution by an inert gas enhances the occurrence of the MILD condition. Szegö et al.[11] as well as Kumar et al.[14] found that air preheating is not required to achieve MILD combustion. Szegö et al.[11] claimed that a certain threshold of the fuel/air momentum ratio G_f/G_a ($\approx$0.006 for their test system) is necessary for the MILD combustion to occur. This momentum rate was considered to ensure the penetration of the fuel jets to a region classified as the oxidation zone. However, they did not systematically investigate the correlation of MILD combustion with fuel or air injection conditions and burner geometric configuration, which can be realized by varying the air−fuel separation (S) and the fuel/air momentum ratio (G_f/G_a) through changing jet-nozzle diameters (D_f and D_a).

Mi et al.[15,16] used a different burner configuration at the same furnace as in refs 11 and 12 to investigate the effects of the air−fuel injection momentum rate and premixing on the MILD combustion. These authors carried out the investigation both experimentally and by numerical simulation. Some of the simulations by Mi et al.[15,16] were verified using their own experiments. A number of different patterns of partially and fully premixed reactants were found to work very well for MILD combustion. Their numerical study suggested that there is a critical momentum rate of the inlet fuel−air mixture, below which the MILD combustion does not occur. In the MILD regime, both the inlet fuel−air mixedness and momentum rate impose insignificant influence on exhaust emissions of the MILD combustion. It is worth noting that their fuel and air jets issued separately from a central and an annulus nozzle (non-premixed) or both from an annulus nozzle (premixed). Later, Li et al.[17,18] further investigated impacts of various particular injection conditions on the characteristics of fully premixed MILD combustion from a single jet burner in the same furnace. The injection conditions include the diameter of the nozzle (D), equivalence ratio (ϕ), thermal input (P), and initial dilution of reactants (f). They showed that all of these parameters have significant influence on the MILD combustion. Also, the premixed combustion was found to occur

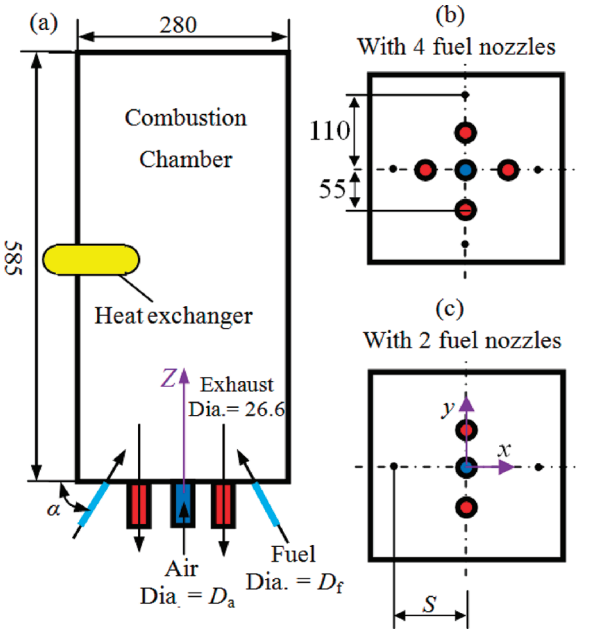

Figure 1. Schematic diagram of the MILD combustion furnace system for present simulations.

only when the injection Reynolds number exceeds its critical value. Moreover, very low emissions of NO_x, CO, and H_2 were measured for the premixed MILD combustion under various conditions.

In this context, the present study was assigned to investigate by Reynolds-averaged Navier−Stokes (RANS) equation modeling the influence of initial injection conditions of fuel and air streams on combustion, mainly MILD, characteristics at the same furnace as for Szegö et al.[11,12] The main objective is to examine the relative effects of seven independent parameters of operation, namely, the mass fraction (f) of fuel diluents (CO_2 and N_2), air preheat temperature (T_a), global equivalence ratio (ϕ), air nozzle exit diameter (D_a), fuel nozzle exit diameter (D_f), fuel−air initial separation distance (S), and fuel injection angle from the furnace floor (α). More specifically, the present investigation aims to quantify the influences of the seven parameters on two variables: the downstream distance of the confluence point of initially fuel and air jets or the fuel-jet penetration distance from the burner exit (Z_J) and the internal recirculation rate of the exhaust gas relative to the total reactant mass flux (K_v). Note that the values of Z_J and K_v are very hard to obtain from experiments.

2. COMPUTATIONAL DETAILS

2.1. Furnace Configuration and Reference Conditions. The RANS modeling presented in this paper is concerned with different reacting cases, mainly operating in the MILD mode, including some tested experimentally by Szegö et al.[11] The test furnace, a laboratory-scale furnace of 20 kW, is shown in Figure 1, and the detail is given in ref 11. Here, only a brief description is provided. The combustion chamber is square with a cross-section of 280 × 280 mm and 585 mm high. The burner system consists of a central air jet nozzle (diameter = D_a) and four (tested) or two off-axis fuel injectors (diameter = D_f). Combustion air may be preheated to a temperature up to T_a = 723 K by an electric heater. The reference operating conditions for this study are a thermal input of P = 15 kW, an equivalence ratio of ϕ = 0.8, and an air preheat temperature of T_a = 723 K. For the present investigation, NG (85% CH_4 and 15% C_2H_6 by mass) is used for P = 15 kW, and thus, the mass

dx.doi.org/10.1021/ef201161x |*Energy Fuels* 2012, 26, 265–277

Table 1. Furnace Operational Conditions for P = 15 kW

case	operational parameters varying	operational conditions fixed
	Figure 1b: 4 Fuel Nozzles and 4 Exhaust Ports	
1 (reference)	D_f (mm) = 2 and 3	D_a = 26.6, S = 110, T_a = 723 K, and ϕ = 0.8
2 (reference)	f_{N_2} (%) = 0, 20, 33, 50, and 75	D_f = 3, D_a =26.6, S = 110, T_a =723K, and ϕ = 0.8
3 (reference)	f_{CO_2} (%) = 0, 20, 38, 65, and 75	D_f = 3, D_a = 26.6, S = 110, T_a = 723K, and ϕ = 0.8
4 (reference)	ϕ = 0.6, 0.7, 0.75, 0.85, and 0.9	D_f = 3, D_a = 26.6, S = 110, and T_a = 723 K
5	T_a (K) = 288, 373, 523, 723, and 823	D_f = 2, D_a = 26.6, S = 110, and ϕ = 0.8
6	D_a (mm) = 40, 26.6, 16, and 10	D_f = 3, S = 110, T_a = 723 K, and ϕ = 0.8
	Figure 1c: 2 Fuel Nozzles and 2 Exhaust Ports	
7	D_f (mm) = 2, 5, 7, and 9	D_a = 26.6, S = 80, T_a = 723 K, and ϕ = 0.8
8	f_{N_2} (%) = 0, 33, 50, 60, and 67	D_f = 5, D_a = 26.6, S = 80, T_a = 723 K, and ϕ = 0.8
9	S (mm) = 110, 80, 50, and 20	D_f = 5, D_a = 26.6, T_a = 723 K, and ϕ = 0.8
10	α (deg) = 30, 60, 90, 120, and 150	D_f = 5, D_a = 26.6, S = 80, T_a = 723 K, and ϕ = 0.8

Table 2. Global Combustion Mechanism Used for NG with Kinetic Data (Units in SI)[a]

reactions	A	β	E_a (J kg^{-1} mol^{-1})	reaction orders
$CH_4 + 1.5O_2 \rightarrow CO + 2H_2O$	5.012×10^{11}	0	2×10^8	$[CH_4]^{0.7}[O_2]^{0.8}$
$CO + 0.5O_2 \rightarrow CO_2$	2.239×10^{12}	0	1.7×10^8	$[CO][O_2]^{0.25}[H_2O]^{0.5}$
$CO_2 \rightarrow CO + 0.5O_2$	5×10^8	0	1.7×10^8	$[CO_2]$
$C_2H_6 + 3.5O_2 \rightarrow 2CO_2 + 3H_2O$	6.186×10^9	0	1.256×10^8	$[C_2H_6]^{0.1}[O_2]^{1.65}$

[a] The reaction rate coefficient = $AT^{\beta}\exp(-E_a/R_uT)$, where R_u is the universal gas constant (=8315 J kmol^{-1} K^{-1}).

flow rates of air and fuel are $\dot{m}_a \approx 6.272 \times 10^{-3}$ kg/s and $\dot{m}_f \approx 2.93 \times 10^{-4}$ kg/s, respectively.

Table 1 lists all cases considered in the present study for the power rate P = 15 kW. Note that numerical tests were performed by varying T_a, D_a, D_f, or S in the second column at the listed values when keeping constant those parameters in the third column of the table. Cases 1−4 were investigated experimentally by Szegö et al.[11] and, hence, are referred to as reference cases. Note that the variation of the fuel/air momentum ratio G_f/G_a was achieved by changing the variables of cases 1−8.

2.2. Computational Conditions and Models. The commercial computational software package Fluent 6.3[22] was used for the present modeling study. Full three-dimensional structured grids were constructed to have small orthogonality deviations. A similar grid resolution study to that of Li et al.[17] was performed to achieve grid-independent results. Three different mesh sizes, which contained about 0.5, 1.0, and 2.0 million hexahedral and tetrahedral cells, were tested. On the basis of comparisons of velocity and temperature profiles between the three meshes for reference operating conditions, the mesh with 1.0 million cells was selected. The finest mesh showed only marginal improvements for a much higher computational cost.

All fuel, air, and flue gas were assumed to obey the ideal gas law. Their specific heats were represented as a function of the temperature (piecewise polynomial).[23] Inlet, outlet, and wall boundary conditions of the computational domain were set as constant velocity, constant static pressure (1.0 atm), and constant temperature boundaries, respectively.

The standard $k-\varepsilon$ model with the standard wall function was used for modeling the turbulent flow. The eddy dissipation concept (EDC) with three-step chemical kinetic mechanisms for CH_4 and one-step mechanism for C_2H_6 were applied (see Table 2) rather than a detailed GRI-3.0 mechanism. Li et al.[17] examined the suitability of the global chemical kinetic mechanism for the MILD combustion in the furnace of the present investigation. Their preliminary simulations for a premixed case were carried out for the EDC model with the global mechanism and with a detailed GRI-3.0 mechanism. Checks were made to differences in the mean temperature (T) and concentrations of CO_2 and O_2 (Y_{CO_2} and Y_{O_2}) obtained from using the two mechanisms. These authors demonstrated that all of the distributions of T, Y_{CO_2}, and Y_{O_2} are in good agreement for the two mechanisms. Also, the EDC model with both reaction mechanisms predicted well the in-furnace temperature and concentrations of CO_2 and O_2 against the experimental data. Accordingly, the global mechanism was used for all of the present simulations to reduce the computational time and make the simulations with the three-dimensional furnace affordable.

Moreover, the present calculation adopted the *in situ* adaptive tabulation (ISAT) model by Pope[23] to reduce the computational cost of integration. The discrete ordinate (DO) radiation model[24] with the weighted sum of gray gas model (WSGGM) to model the gas emissivity was applied for radiation. The SIMPLE algorithm was used for pressure velocity coupling.

A second-order discretization scheme was used to solve all governing equations. Convergence was obtained when the residuals are less than 10^{-6} for energy and DO intensity and 10^{-5} for all other variables. The outlet temperature was monitored, and its variation within 1 K was allowed for convergence of the solution.

3. RESULTS AND DISCUSSION

To verify the present simulations, we first make comparisons between present numerical predictions and previous measurements by Szegö et al.[11,12] for reference cases 1−4.

3.1. Verification of the Model. *3.1.1. Mean Velocity.* Panels a−d of Figure 2 compare lateral profiles of the axial mean velocity (V_z) at locations z = 60.5 and 176.5 mm with x = 0 and −10 mm for case 1 (D_f = 2 mm, D_a = 26.6 mm, S = 110 mm, T_a = 723 K, and ϕ = 0.8) obtained from the present simulations and the previous laser Doppler anemometry (LDA) measurements.[11,12] Note that, as indicated in ref 12, the lateral velocity component (V_x or V_y) is too small to be measured reliably by LDA, so that only the axial velocity data are presented here for comparison. The profiles near the jet exit plane (z = 60.5 mm) clearly reflect

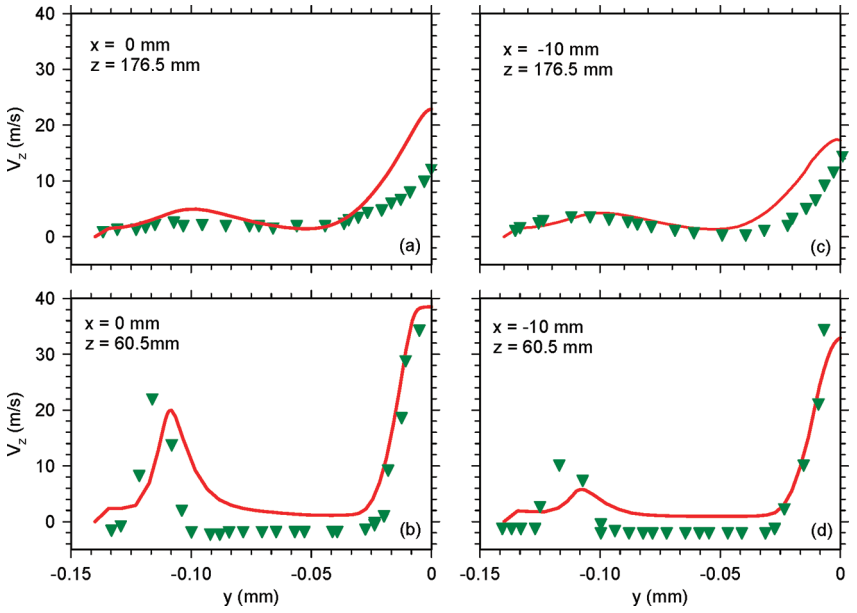

Figure 2. Comparison of the experimental (green ▼) and numerical (red —) axial velocities versus y locations for the baseline case: (a) $x = 0$ mm and $z = 176.5$ mm, (b) $x = 0$ mm and $z = 60.5$ mm, (c) $x = -10$ mm and $z = 176.5$ mm, and (d) $x = -10$ mm and $z = 60.5$ mm.

the presence of the central air jet and side fuel jets. It is also evident that the certain distance between different nozzles prevent the air and fuel jets from mixing with each other in the region near the nozzle exit plane. The axial velocities measured were close to zero or even slightly negative in the near-nozzle region between the fuel jets and the air jet, likely because of the presence of the downward exhaust streams. Unfortunately, also, the inlet velocity profile of the central air jet measured was not symmetrical, as noted by Szegö.[12] It follows that the downstream flow field must be asymmetric as well. This can actually be observed from the evolution of the measured velocity profiles shown in Figure 2. Such asymmetries certainly cannot be captured by the present simulation because all inlet profiles of the velocity, temperature, and concentrations for the simulation were set to be uniform or symmetrical. Note that those profiles were impossibly measured by Szegö,[12] so that no detailed inlet velocity profiles were given even for some non-reacting cases.

Indeed, some obvious differences occur between the predicted and measured velocity profiles. The modeling prediction of the fuel-jet velocity is lower by up to 10% at $x = 0$ but performed well for the air jet at $z = 60.5$ mm. By comparison, it appears that the overall performance of the modeling is poorer farther downstream at $z = 176.5$ mm. However, overall, it is fair to say that there is qualitatively reasonable agreement between the CFD calculations and the LDA data for reacting conditions, which means that the in-furnace flow structure is reasonably captured by the modeling, in a qualitative sense.

3.1.2. Mean Temperature. Panels a−c of Figure 3 show lateral distributions of the mean temperature at three different axial locations (z = 42.5, 142.5, and 442.5 mm) and yz planes, obtained for case 1 from the numerical simulation and experimental measurements. The large variation in the temperature at the lower part of the furnace is induced by the inlet nozzle streams of the different reactants and the exit ports of the hot combustion products. The agreement with the model at the lower location is fair, and the differences can a function of the uncertainty in measuring the initial conditions or accurately capturing the flow dynamics.

In the upper part of the furnace (e.g., $z = 442.5$ mm), the mean temperature is predicted well, consistent with the measurements and the low temperature gradient expected in MILD combustion conditions. Therefore, it can be deduced that MILD combustion was reproduced numerically for case 1.[12]

The mean temperatures for cases 2−5 were also compared to the model results. In ref 10, the temperature measured at $z = 542.5$ mm and on the furnace axis is considered as the furnace temperature, denoted here by T_c. Present predictions of this temperature versus T_a and ϕ for cases 4 and 5 are shown in panels a and b of Figure 4, respectively, for comparison to the measurements.[11] Included in Figure 4b is also the exhaust CO_2 versus ϕ. Evidently, the present predictions of the mean temperature and the exhaust CO_2 agree quite well with the experimental results. The furnace temperature grows slightly with increasing preheat and also with decreasing excess air, i.e., increasing ϕ. However, the growth rate of T_c (and also NO_x; see ref 11) is much lower than that of T_a. This suggests that both T_a and ϕ are not a strong factor influencing the MILD combustion. It is also clear that the model capturing the heat loss from the furnace through the heat exchanger and walls is well-predicted.

Figure 4a also shows the furnace temperature (T_c) against the mass fraction of N_2 and CO_2 injected as a diluents with the fuel (f_{N_2} and f_{CO_2}). As expected, the furnace temperature drops with increasing f_{N_2} or f_{CO_2} in the fuel stream. Evidently as well, the predictions compare quite well to the experiments, allowing uncertainties from both the experiments and calculations.

With all of the evidence shown above taken into consideration, we were able to conclude that the RANS modeling approach is capturing all of the main features of these flames and is appropriate to investigate the influence of initial injection conditions of fuel and air streams on the global characteristics of the combustion in this furnace.

3.2. Dependence of the Thermal and Flow Fields upon Various Parameters. To visualize global changes of the mean

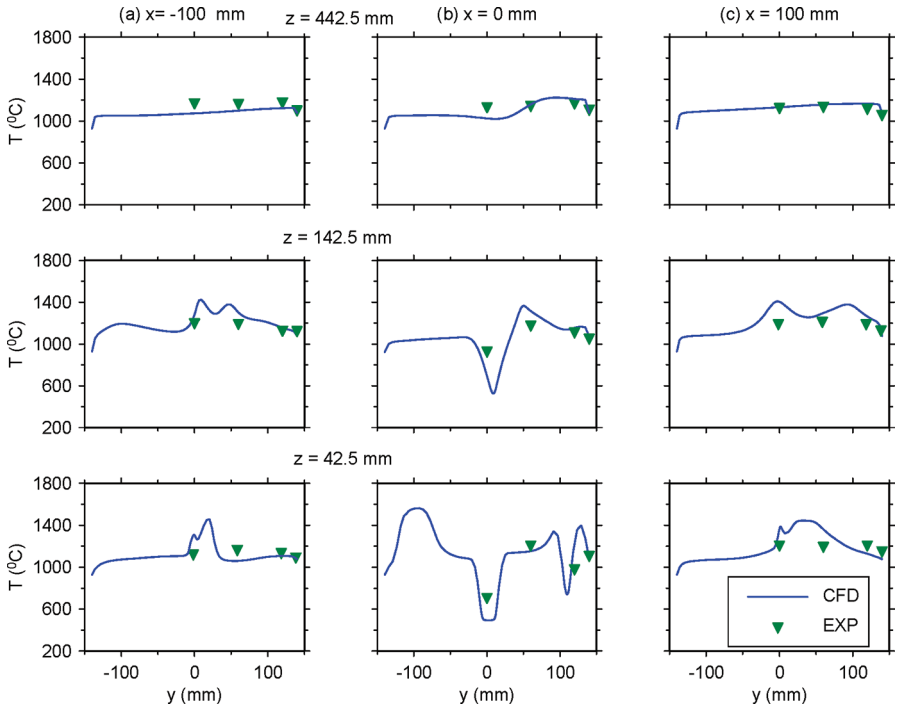

Figure 3. Comparison of the experimental and numerical mean temperature profiles along the y axis at $x = -100$ (left), $x = 0$ (center), and $x = 100$ (right) for $z = 42.5$, 142.5, and 442.5 mm (case 1).

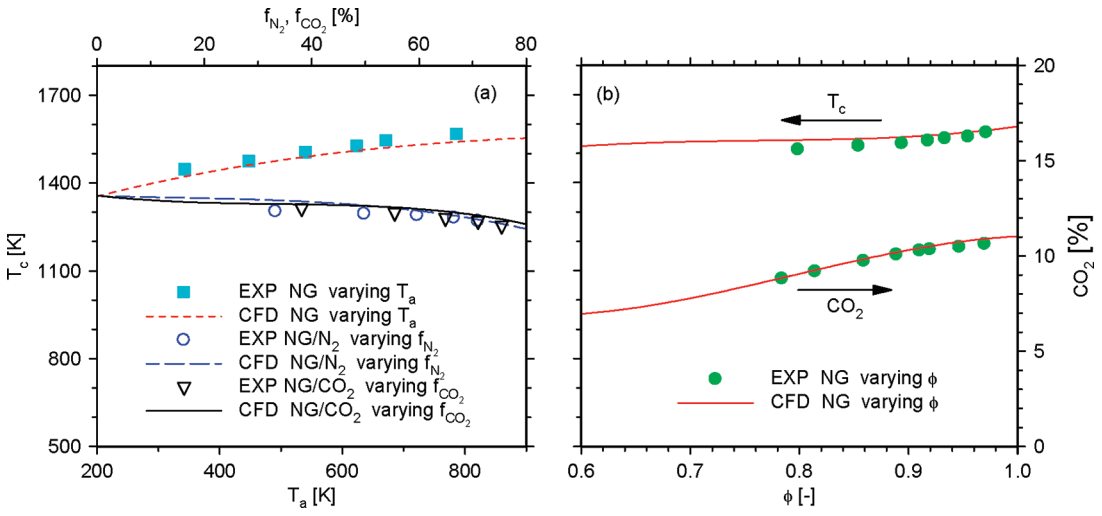

Figure 4. Centerline mean temperature (T_c) at $z = 542.5$ mm versus (a) air preheat temperature (T_a)/diluent mass fractions (f_{N_2} and f_{CO_2}) and (b) equivalence ratio (ϕ). Also included in panel b is the exhaust CO_2 versus ϕ. Experimental data are reproduced from Figures 4–10 by Szegö et al.[11]

velocity (U) and temperature (T) fields with varying the operational parameters, panels a–f of Figures 5 and 6 display the U and T contours at the central xz plane ($y = 0$), respectively, obtained for cases 2, 5, 6, 7, 9, and 10. As seen from panels a–f of Figure 6, flow patterns for all of these cases are similar and can be simplified by a schematic drawing in Figure 7, adopted from Szegö et al.;[11] i.e., these flows are all characterized by a central upward stream ($U > 0$) and the downward (flue-gas) streams ($U < 0$) mainly through the four furnace corners, which can be shown by the cross-sectional velocity contours (not presented). For all of the cases, except for $\alpha = 120°$ and 150° of case 10, as z increases, the "weak" fuel jets are "dragged" by and, hence, inclined to the "strong" central jet. Before the reactant jets "meet" at their junction point, each jet has entrained a certain quantity of hot combustion products, so that they have been diluted and also heated. If, because of changing some parameter(s), both dilutions of oxidant and fuel become sufficient at their junction point where the local temperature of the gaseous mixture is above the point of autoignition of the fuel, the stable MILD combustion is expected to take place, so that the mean temperature distribution in the upper part of the furnace becomes more uniform. Otherwise, if the dilutions are insufficient, e.g., for $\alpha = 30°$ and 60° (case 10) and $S = 20$ and 50 mm (case 9), a more conventional flame is expected and a higher peak

dx.doi.org/10.1021/ef201161x |*Energy Fuels* 2012, 26, 265–277

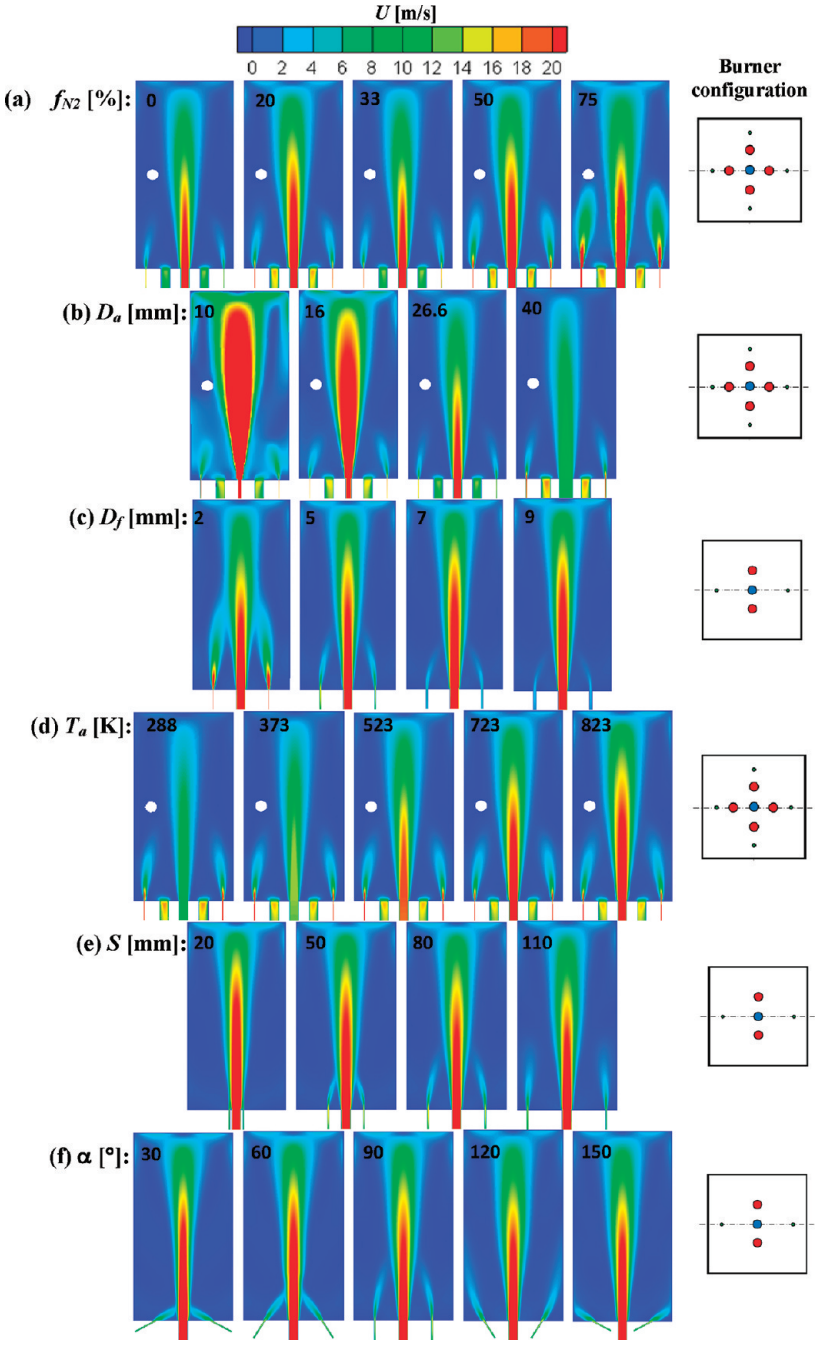

Figure 5. Calculated mean velocity contours at the central *xz* plane ($y = 0$) for cases 2, 5, 6, 7, 9, and 10.

temperature is predicted. The mean temperature contours in panels a−f of Figure 6 appear to point to the above deductions.

More specifically, in case 1 (reference), the MILD combustion occurs for $D_f = 2$ mm (see[11]), so that the temperature distribution is quite uniform. When D_f is increased from 2 to 3 mm, the injection speed of fuel jets at the same mass flux as for $D_f = 2$ mm is decreased by 125% and, thus, the fuel momentum rate is decreased significantly. This consequently leads to less dilution of the fuel before entering the main reaction zone. As a result, the measured flame often becomes visible randomly in space, called "ghost flames" by Szegö et al.,[11] and the predicted maximal mean temperature increases noticeably from $T_{max} \approx 1686$ to 1800 K (note that the maximum mean temperature T_{max} should be a key parameter reflecting MILD combustion because it is a measure of the uniformity of the mean temperature and also the NO_x emission). Similar observations can also be made for case 7. That is, as D_f is increased from 2 to 9 mm, the junction point shifts upstream (downward; see Figure 5c) and the difference between the peak temperature and the flue-gas temperature reduces (Figure 6c). Note that different burner configurations are used for cases 1 and 7, as shown by panels b and c of Figure 1, respectively. While the nozzle dimension and configuration cannot be varied during operation, the reduction in jet momentum and, hence, penetration because of large fuel nozzle diameters can be addressed by premixing the fuel with inert gas, such as nitrogen (N_2) or carbon dioxide (CO_2), and, thus, increasing

dx.doi.org/10.1021/ef201161x |*Energy Fuels* 2012, 26, 265–277

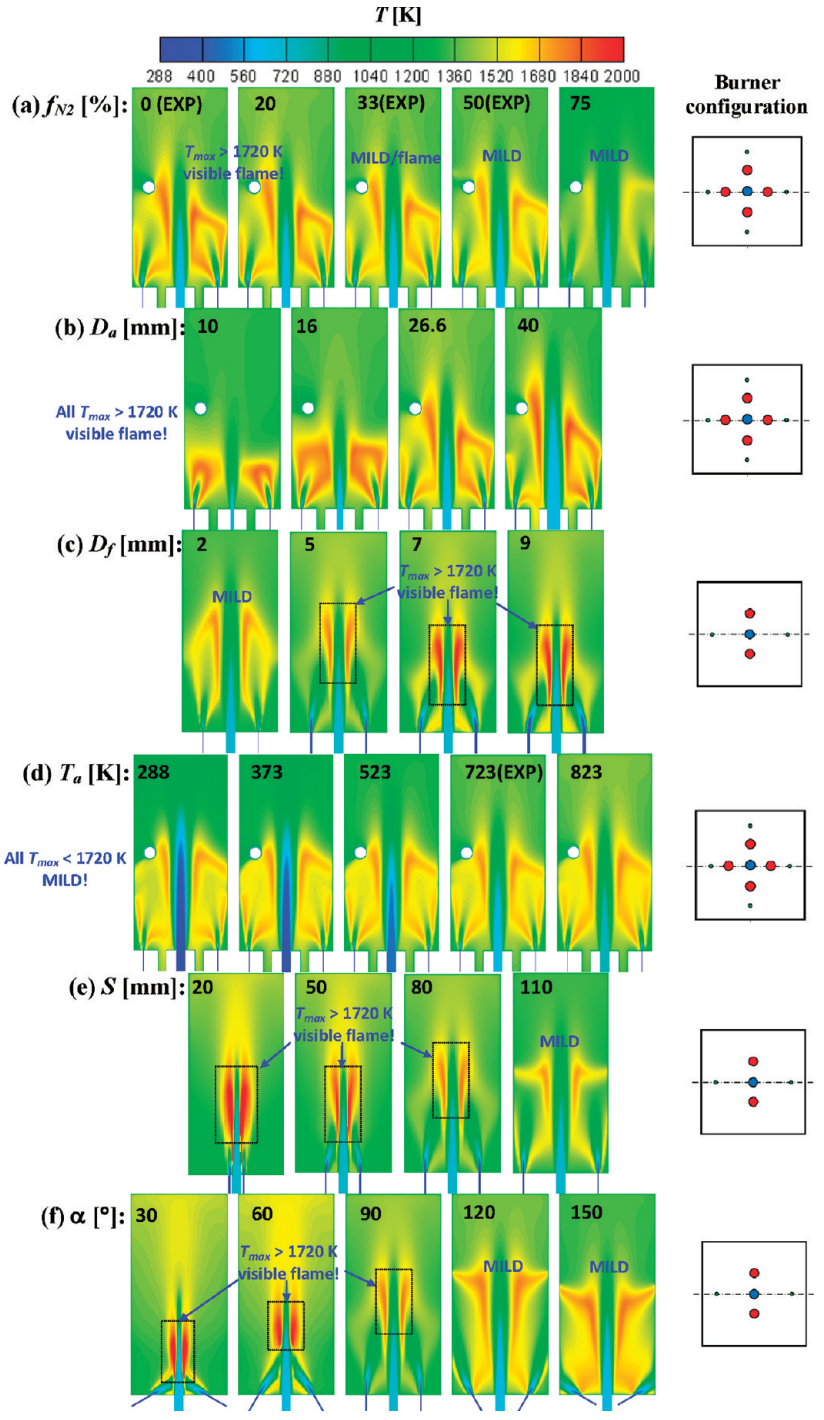

Figure 6. Calculated mean temperature contours in the central *xz* plane for cases 2, 5, 6, 7, 9, and 10.

the fuel momentum rate. Indeed, when the fuel through the 3 mm nozzles was premixed with N_2 at $f_{N_2} \geq 50\%$, Szegö et al.[11] could completely restore the stable MILD combustion and, thus, make a more uniform temperature field. Our simulation has resulted in the similar behavior for cases 2 (see Figure 6a), 3, and 8. This is well-understood because the initial dilution leads the fuel jets to have a higher injection momentum rate, so that their mixing with the central oxidant jet is delayed or their confluence point shifts downstream. Hence, a sufficiently high rate of the fuel injection momentum is critical for the MILD combustion to occur.

Upon plots of panels a−f of Figure 6, the combustion status is marked by "MILD" or "visible flame" based on the maximal temperature T_{max} = 1720 K or 1450 °C. This "critical" value derives from comparisons of the predicted values of T_{max} to the experimental observations by Szegö et al.[11] for the reference cases of diluting fuel through the 3 mm nozzles, i.e., cases 2 and 3. Szegö et al.[11] observed that, when f_{N_2} = 33% or f_{CO_2} = 38%, the measured combustion was very occasionally visible with tiny flame spots; see their sequence of instantaneous images of NG combustion with increasing N_2 and CO_2

dx.doi.org/10.1021/ef201161x |*Energy Fuels* 2012, 26, 265–277

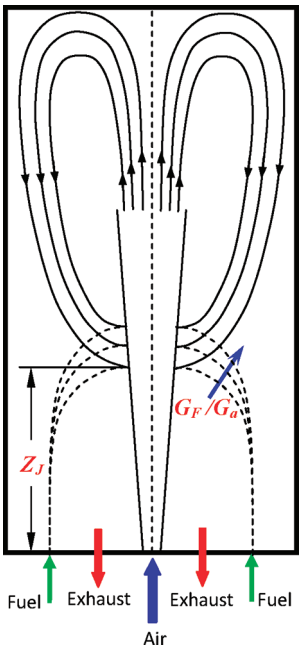

Figure 7. Schematic of the symmetric representation of the simplified aerodynamics inside the furnace, modified from ref 11.

dilution (their Figure 8). Such combustion should be considered critical in transition from the traditional to MILD mode. Our calculations obtained that $T_{max} \approx 1710-1720$ K for these cases with $f_{N_2} = 33\%$ and $f_{CO_2} = 38\%$. It follows that the critical value of T_{max} is determined as 1720 K. We also checked other cases for which Szegö et al.[11] measured and validated this value.

Fundamentally, both the effects of f_{N_2} (or f_{CO_2}) and D_f should be considered as the result of varying the fuel injection momentum rate G_F (with the subscript "F" relating to the diluted fuel jet), which can be expressed as

$$G_F = \frac{4\dot{m}_F^2}{\pi\rho_F D_f^2} \propto \frac{4\dot{m}_F^2 T_F}{\pi D_f^2} \quad (1)$$

where T_F and ρ_F are the initial diluted fuel temperature and density, respectively. One would then ask whether a change to the air momentum rate

$$G_a = \frac{4\dot{m}_a^2}{\pi\rho_a D_a^2} \propto \frac{4\dot{m}_a^2 T_a}{\pi D_a^2} \quad (2)$$

by varying D_a and T_a (and even ϕ, despite changing the initial fraction of O_2) can lead to similar outcomes. Certainly, a variation of D_a changes the in-furnace flow velocity field and temperature field; see Figures 5b and 6b. However, the combustion state does not appear to vary between the traditional and MILD modes when varying D_a, indicating a difference between the effects of D_a and D_f. Increasing D_a results in an opposite shift of the junction point from that by increasing D_f. Namely, the junction point moves downstream (upward) as D_a is increased or G_a is decreased. It is also apparent that an increase in D_a yields a greater reaction zone, which differs, as well, from that caused by increasing D_f. The above opposite trends can be unified when considering the fuel/air momentum ratio, viz.

$$\frac{G_F}{G_a} = \frac{\rho_a}{\rho_F}\left(\frac{\dot{m}_F}{\dot{m}_a}\right)^2\left(\frac{D_a}{D_f}\right)^2 = \frac{\phi^2}{\gamma_s^2(1-f)^2}\left(\frac{T_F}{T_a}\right)\left(\frac{D_a}{D_f}\right)^2 \quad (3)$$

where γ_s is the stoichiometric air/fuel ratio. Equation 3 indicates that G_F/G_a increases with increasing D_a but with decreasing D_f. Hence, if increasing G_F/G_a results in the jet confluence point shifting downstream, then increasing D_a or decreasing D_f will do the same, which then enables the main reaction zone to move upward and become larger in size (panels b and c of Figure 6), so that the mean temperature is more uniform. By comparison, the decrease of G_F/G_a by increasing T_a does not appear to shift the confluence location (see Figure 5d) but reduces the mean temperature difference slightly (Figure 6d). Note that the MILD combustion occurs for all tested values of T_a, in this case where $D_f = 2$ mm.

Different from the above parameters, the separation between the fuel and air exits (S) and the injection angle (α) of the fuel jet from the furnace floor, two critical parameters that perhaps can control the establishment of MILD combustion, are not related to the momentum ratio G_F/G_a. Increasing either S or α will shift the confluence point further from the jet exits and, therefore, enable each jet to entrain more combustion products prior to entering the main reaction zone. It follows that the combustion reaction will take place at a lower rate, leading to the flame temperature or the maximum temperature T_{max} dropping. Indeed, this can be observed from panels e and f of Figure 6. Furthermore, the conventional visible flame must occur either for case 9 when $S = 20$ and 50 mm, with $T_{max} \approx 1940$ and 2200 K, or for case 10 when $\alpha = 30°$ and 60°, with $T_{max} \approx 2188$ and 1988 K, because these flame temperatures (>1720 K) are too high. By comparison, for $S = 110$ mm or $\alpha = 120°$ and 150°, the flame temperatures are considerably lower ($T_{max} = 1629$ or 1708 and 1713 K, respectively), so that the MILD combustion should occur as indicated in panels e and f of Figure 6.

3.3. Effects of Different Operational Parameters on the Fuel-Jet Penetration (Z_J) and the Relative in-Furnace Recirculation Rate (K_v). Panels a–f of Figures 5 and 6 demonstrate that variations of all seven parameters of the present investigation affect the diffusion flame characteristics expressed by the in-furnace velocity and temperature distributions. However, these plots cannot show quantitatively the extent of the influence from each parameter and especially cannot determine the location of confluence between the reactant jets or the fuel-jet penetration distance from the burner exit (Z_J), an important quantity for describing the MILD combustion, as discussed by Szegö et al.[11] and Grandmaison et al.[26] It should be significant to quantify the effects of all of the parameters on the confluence location Z_J. Moreover, the recirculation rate of the exhaust gas is also important for the establishment of MILD combustion, and therefore, its value relative to the total reactant mass flux at the confluence point (K_v) should be estimated. Nevertheless, it is worth noting that the magnitudes of Z_J and K_v (see their definitions below) are highly difficult or even impossible to obtain by experiment.

3.3.1. Definitions of the Fuel-Jet Penetration and Relative Recirculation Rate. Fuel-jet penetration (Z_J): When the fuel and oxidant streams/jets discharge separately into the furnace, their direct mixing occurs after their confluence at a certain distance downstream from the burner exit (see Figure 7). This distance is termed herein as the fuel-jet penetration, denoted by Z_J. In the present paper, Z_J is defined to be the minimum value of z at which

dx.doi.org/10.1021/ef201161x |*Energy Fuels* 2012, 26, 265–277

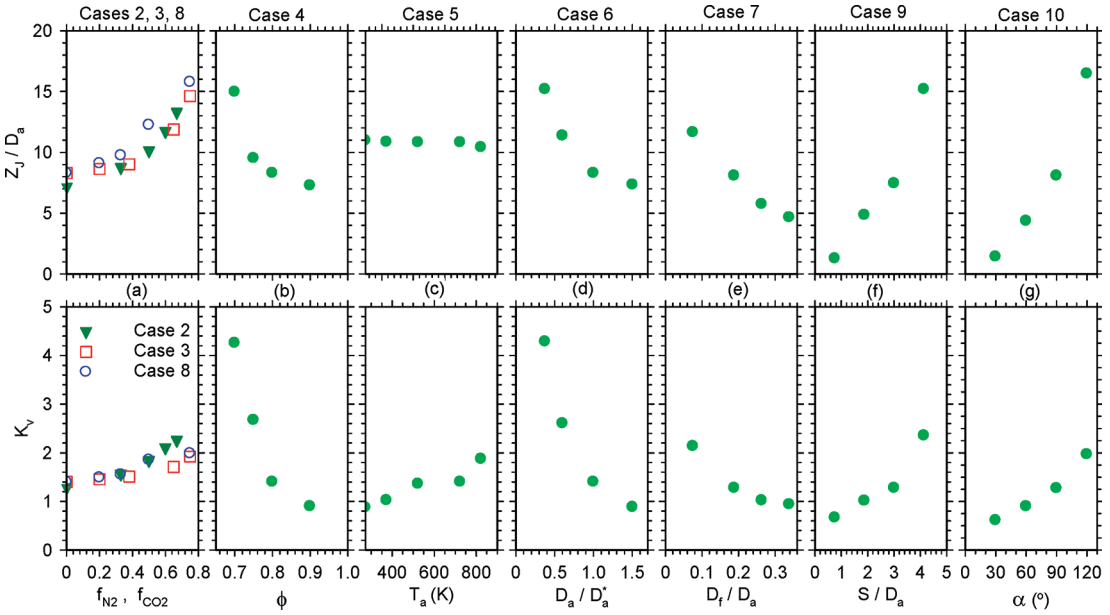

Figure 8. Calculated Z_J and K_v plotted versus different parameters f, T_a, ϕ, D_a, D_f, S, and α. Note that the horizontal axis of panel d is normalized by D_a^* = 26.6 mm because D_a varies in case 6; for all other cases, the constant air nozzle diameter D_a = 26.6 mm.

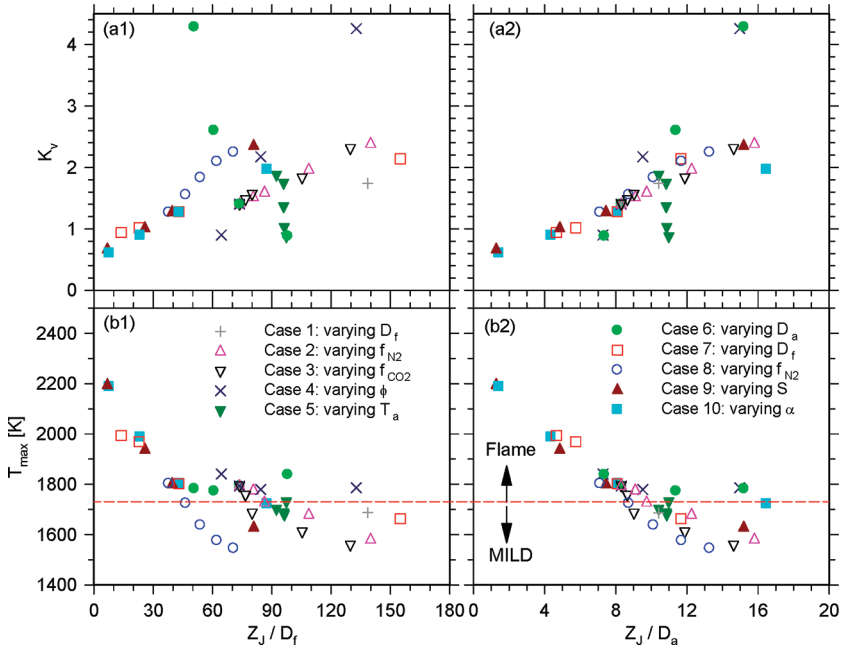

Figure 9. Calculated K_v and T_{max} for all of the cases plotted against the normalized penetration distance Z_J.

only the central peak of the axial component of the mean velocity (V_z) exists across the central yz and xz planes.

Relative recirculation rate (K_v): The intense dilution of reactants prior to their combustion reactions is one of the vital requirements for achieving overall MILD combustion in the downstream region at $z \geq Z_J$. The degree of dilution occurring at $z = Z_J$ may be measured by the relative recirculation rate, viz.

$$K_v = \dot{m}_r/(\dot{m}_a + \dot{m}_f) \quad (4)$$

which was defined first by Wünning and Wünning.[1] Here, $\dot{m}_r$ and $(\dot{m}_a + \dot{m}_f)$ denote, respectively, the total recirculated mass flow rate of the exhaust gas entrained by air and fuel jets and the mass flow rate of the injecting reactants (i.e., air and fuel). The present $\dot{m}_r$ may be obtained from

$$\dot{m}_r = \dot{m}_e + \dot{m}_i = \dot{m}_{up} - (\dot{m}_a + \dot{m}_f)$$

where $\dot{m}_i$ and $\dot{m}_e$ are the mass fluxes of internal exhaust gas and external diluents, respectively, while $\dot{m}_{up}$ represents the upward mass flow rate at $z = Z_J$, viz.

$$\dot{m}_{up}(Z_J) = \iint_{A(Z_J)} \rho v_z(x,y)\mathrm{d}x\mathrm{d}y \quad (5)$$

dx.doi.org/10.1021/ef201161x |*Energy Fuels* 2012, 26, 265–277

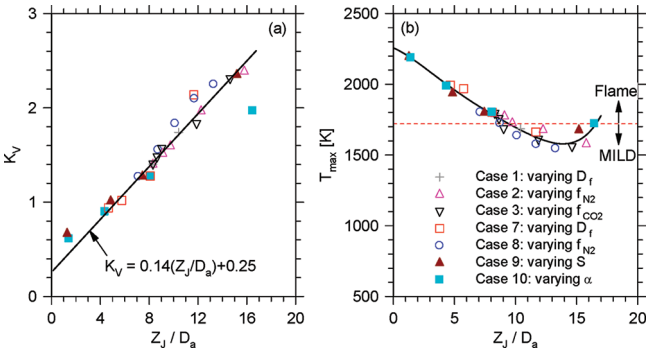

Figure 10. Influences of Z_J on K_v and T_{max} for cases 1−3 and 7−10.

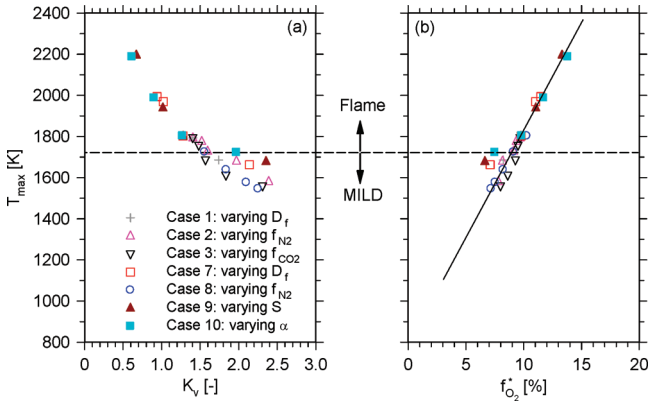

Figure 11. Calculated mean T_{max} plotted versus K_v and f_{O_2} (the overall O_2 concentration before the reaction) measured at the junction point of the reactant jets for cases 1−3 and 7−10.

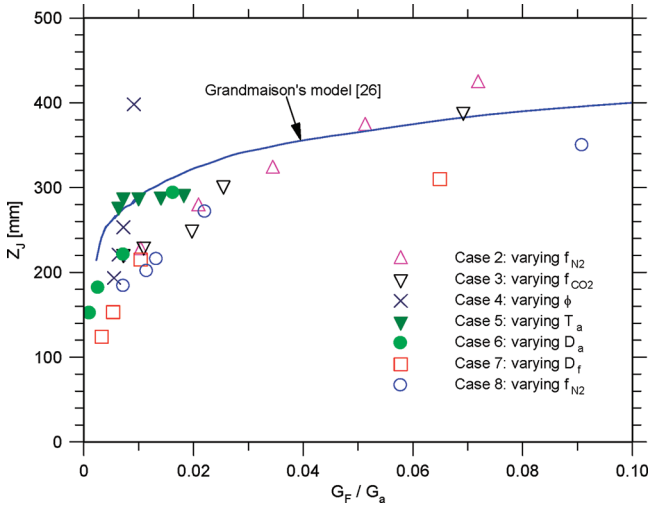

Figure 12. Penetration distance Z_J plotted versus the fuel/air momentum ratio G_F/G_a.

with $A(Z_J)$ being the area with $v_z > 0$. For the same total inlet mass flow rate of reactants, a higher value of $\dot{m}_{up}(Z_J)$ reflects a higher entrainment rate of the exhaust gas and, thus, a greater recirculation rate.

3.3.2. Effects of Different Parameters on Z_J and K_v. Dependences of Z_J and K_v on the seven parameters, i.e., f, T_a, ϕ, D_a, D_f, S, and α, are quantified using the present velocity data from the model and plotted in panels a−g of Figure 8. Clearly, both Z_J and K_v increase significantly as either f, S, or α is increased but, in general, decrease with increasing the other parameters. Among all of the parameters, the fuel-jet separation from the air jet (S) and the fuel-jet angle from the floor (α) are obviously the most effective parameters that affect the penetration distance Z_J. On the other hand, the parameters ϕ and D_a appear to be most influential for changing the relative recirculation rate K_v. By comparison, the combustion air preheat temperature (T_a) is the most ineffective parameter in changing Z_J. T_a also has only a limited influence on the magnitude of K_v. It is thus deduced that the preheat is not vital for the MILD combustion to occur. This is consistent with the finding by Schaffel-Mancini et al.,[19] who noted that the impact of the combustion air temperature on the performance of the coal-fired boiler is not critical if the intensive in-furnace recirculation has been created for MILD combustion.

Some comments may be useful on the effect of the fuel/air momentum ratio G_F/G_a in relation with the results of panels a−f of Figure 8. Equation 3 shows that G_F/G_a is a function of f, T_F, T_a, ϕ, D_a, and D_f and independent of S and α. It also indicates that the momentum ratio increases with increasing f, ϕ, T_F, and D_a but decreases with enlarging T_a and D_f. This statement has been indirectly confirmed by panels a−f of Figure 8 through the Z_J variations with the parameters; note that Z_J increases with G_F/G_a. However, some explanation for the data of Figure 8d with respect to D_a (case 6) is required. The decrease of Z_J/D_a with increasing D_a might not be expected but is true because of D_a being a variable and acting as the denominator in Z_J/D_a. In fact, Figure 5b shows that, as D_a and, thus, G_F/G_a is increased, Z_J increases significantly, which is totally consistent with eq 3.

Moreover, Figure 8 appears to show that K_v cannot be increased very effectively by manipulating the fuel jets only for the present burner−furnace system. This is understood because the global recirculation rate relies predominately on the "strong" entrainment of the central air jet (the small fuel jets can contribute only a small portion to the magnitude of K_v). However, the occurrence of MILD combustion certainly does not require too large of a value of K_v, as will be argued below.

3.3.3. Effects of Z_J on K_v and the Flame Temperature. Now let us examine the effects of Z_J on K_v and T_{max}. The results obtained from varying all of the parameters are presented in panels a1 and b1 and a2 and b2 of Figure 9 with the normalization of Z_J by D_f and D_a, respectively. Clearly, the normalization by D_a is a better choice. This appears to suggest that, to make a meaningful comparison for different cases, the normalization of Z_J by D_a is essential because the initial momentum rate of the central air jet is much higher than that of the fuel jets and, thus, dominates the in-furnace flow structure. It is evident that, in general, as Z_J/D_a increases, K_v increases, whereas T_{max} decreases. Namely, the low value of T_{max} corresponds to high K_v and vice versa. Panels a2 and b2 of Figure 9 indicate that different data sets for either K_v or T_{max} do not collapse onto a single curve. In particular, the data related to T_a, ϕ, and D_a of the central air jet behave distinctly. Modifications of these three parameters change T_{max} insignificantly (1629−1840 K) but change K_v drastically (0.88−4.3). This may suggest that changes to the initial conditions relating to the central air jet are not quite effective in modifying the combustion characteristics. Nevertheless, it is quite interesting that variations of ϕ and D_a appear to produce a similar correlation between K_v and Z_J/D_a and also between T_{max} and Z_J/D_a.

dx.doi.org/10.1021/ef201161x |*Energy Fuels* 2012, 26, 265–277

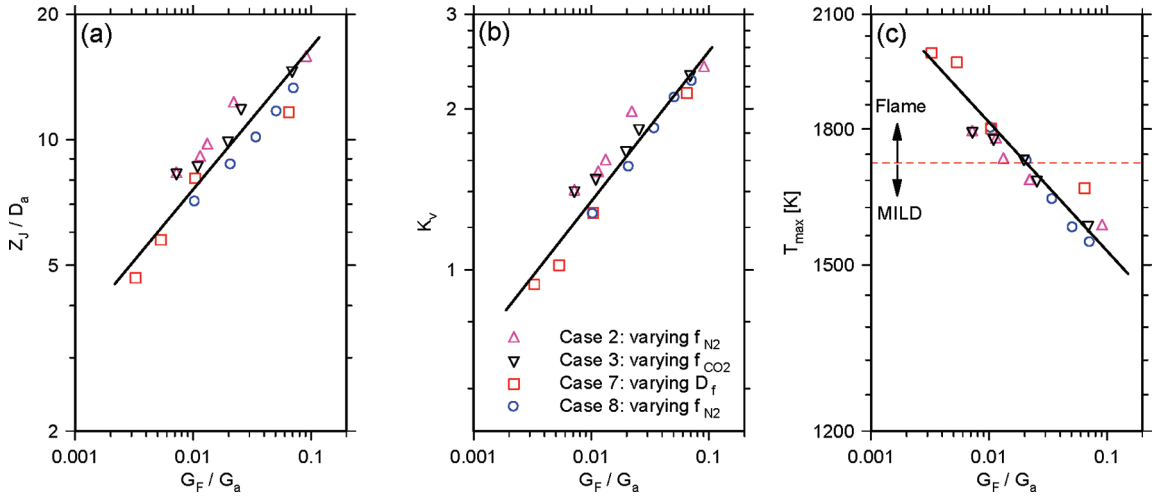

Figure 13. Normalized penetration distance Z_J/D_a, recirculation rate K_v, and maximum mean temperature T_{max} plotted versus the fuel/air momentum ratio G_F/G_a.

When the data for the above three cases (cases 4, 5, and 6) are removed from panels a2 and b2 of Figure 9, the collapsing of all of the rest data, obtained from manipulating the fuel jets or their nozzle arrangement, becomes quite evident (see panels a and b of Figure 10). This finding has practical significance. It indicates that either K_v or T_{max} (reflecting the temperature uniformity) for these flames depends upon Z_J approximately in the same manner, regardless of how Z_J is varied through changing the fuel injection conditions. Although there are many ways to modify a combustor system, the increases of S and α appear to be most effective and efficient for the establishment of MILD combustion; relatively, e.g., the reduction of D_f will require a high gas supply pressure and, thus, more loss of energy, while the dilution of fuel will need to make the system more complex and more expensive. This can be seen from a comparison of the results in panels a and e−g of Figure 8 and points to the importance of vitiation on establishing MILD combustion.

Figure 10 suggests that all of the K_v data for cases 1−3 and 7−10 collapse approximately onto a single line $K_v \approx 0.14 Z_J/D_a + 0.25$, whereas all of the T_{max} data fall roughly along a nonlinear curve. The exception of the K_v data point for $\alpha = 120°$ is not unexpected because they maintain the fuel closer to the exit plane and are not realistic in any practical case (see Figure 5f). Note that the estimate of K_v is impossible for $\alpha = 150°$ because the junction location Z_J cannot be determined.

Panels a and b of Figure 11 show the maximum temperature (T_{max}) against the relative recirculation rate (K_v) and the overall O_2 concentration of the diluted mixture (f_{O_2}) obtained at $z = Z_J$, respectively. Evidently, if it can be achieved by modifying the fuel-jet parameters that $K_v \geq 1.5$ or $f_{O_2} \leq 9\%$ at $z = Z_J$, the MILD combustion should be established with T_{max} below 1723 K (dashed horizontal line). Noteworthy, the MILD combustion is often characterized with low NO_x emissions,[25] and according to Turns,[27] the formation of thermal NO_x is negligible when the flame temperature is below 1450 °C or 1723 K.

4. FURTHER DISCUSSION

According to eq 3, the effects of the parameters f, T_a, ϕ, D_a, and D_f (but not S and α) can all be represented by that of G_F/G_a. Using a strong (oxidant) jet/weak (fuel) jet model, Grandmaison et al.[26] derived a relation between Z_J and G_F/G_a, which then enables the dependences of both Z_J and K_v upon f, T_a, ϕ, D_a, and D_f to be expressed as single functions of G_F/G_a. This relation was used, without any verification, by Szegö et al.[11] for estimates of Z_J against different D_f and f and even different fuels (see their Figure 10c). However, we believe that a check to this relation using the modeling data is necessary. Figure 12 shows the results of Z_J, K_v, and T_{max} against G_F/G_a for cases 2−8. For comparison, the results from the model by Grandmaison et al.[26] is also presented. Note that the present values of Z_J and those calculated from the simplified model[26] may differ because of slightly different definitions of Z_J. Obviously, the model does not work well for the variations of G_F/G_a caused by all f, T_a, ϕ, D_a, and D_f. In particular, it is totally different from the correlations between Z_J and the parameters related to the central air jet (T_a and ϕ). By comparison, the penetration distance can be estimated reasonably well by the model in the forward flow configuration of the furnace.[10]

The discrepancies between the relation by Grandmaison et al.[26] and the present calculation are expected when taking into account the assumptions used for the model. Actually, a simplified case of the air/fuel jet system was considered in the model,[26] where the effect of buoyancy is negligible and the air jet is statistically axisymmetrical. Besides, the furnace model is sufficiently large, so that the jets can be treated as free jets. The simplified model appears to work reasonably well for the forward-flow furnace[10] but is not applicable for the present configuration. Nevertheless, the detailed variation trend of Z_J of the model is overall consistent with those for cases 2, 3, 7, and 8, achieved by modifying the fuel jets. The reason for this can be attributed to the fuel jets being quite weak and developing within the entrainment field of the strong air jet, so that their modification impose little influence on the latter.

Panels a−c of Figure 13 show the results of Z_J/D_a, K_v, and T_{max} against G_F/G_a for cases 2, 3, 7, and 8, in the form of log−log presentations. It appears that the four sets of data for Z_J/D_a, K_v, and T_{max} approximately collapse separately and that they are all correlated with G_F/G_a roughly in the power-law fashion, i.e.

$$Z_J/D \propto (G_F/G_a)^m; \quad K_v \propto (G_F/G_a)^m; \quad T_{max} \propto (G_F/G_a)^m \qquad (6)$$

This is a significant finding as reasoned below. Equation 6 suggests that the K_v stability criterion defined by Wunning and

dx.doi.org/10.1021/ef201161x |*Energy Fuels* 2012, 26, 265–277

Wunning[3] only holds for a fixed furnace/burner arrangement. That is, the critical values of K_v for the MILD combustion depend upon G_F/G_a, S/D_a, and α, hence, on the air−fuel injection conditions. This coincides with the measurement by Szegö et al.[11] Previously without eq 6, to estimate the critical values, *a priori* knowledge of the flow field is required, either through experiments or numerical modeling. However, the mass flow rate of recirculating combustion products is often difficult to accurately determine in complex combustion chambers. On the other hand, with eq 6, the momentum ratio G_F/G_a, the separation S/D_a, and injection angle α are straightforward parameters to determine and can be used to characterize the MILD combustion processes for a given geometric configuration.

Thus far, the present work has investigated the effects of the operational and geometric parameters (f, T_a, ϕ, D_a, D_f, S, and α) on the in-furnace diffusion combustion of NG injected through four off-axis holes and with air injection through a central nozzle (see Figure 1). The MILD combustion can be well-established in the burner−furnace system of this configuration, as shown experimentally by Szegö et al.[11,12] Significantly, it has been found that the effects of the inlet or "external" parameters f, T_a, ϕ, D_a, and D_f can be expressed as that of G_F/G_a by eq 3, while the in-furnace or "internal" parameters Z_J/D_a, K_v, and T_{max} are correlated with G_F/G_a approximately by eq 6. Dally et al.[28,29] experimentally proved that the MILD combustion can occur in the same furnace, however, with injecting fuel from the central nozzle and air through the four off-axis holes. In such a configuration, eq 3 still works for the ratio G_F/G_a, but effects of G_F/G_a should be opposite to those with respect to the present configuration.

5. CONCLUSION

This study has performed a numerical investigation on the characteristics of MILD combustion in a recuperative furnace, in which reactants and exhaust ports are all mounted on the same wall. The effect of different geometrical and operating parameters on vitiation and establishment of MILD combustion has been presented. These parameters include the mass fraction (f) of fuel diluents (CO_2 and N_2), air preheat temperature (T_a), equivalence ratio (ϕ), air nozzle exit diameter (D_a), fuel nozzle exit diameter (D_f), initial fuel−air separation distance (S), and fuel injection angle from the furnace floor (α). These data have been used to investigate the resulting penetration distance, the impact on internal recirculation and, hence, vitiation, and the maximum mean temperature of the MILD flame.

To verify the suitability of the CFD model and initial and boundary conditions, a comparison was made to the mean velocity and temperature distributions for selected reference cases measured by Szego et al.[11,12] The model was found to agree reasonably well with published experimental data. The modeling study has demonstrated that varying each of the inlet parameters f, T_a, ϕ, D_a, D_f, S, and α can considerably influence the fuel-jet penetration distance, the recirculation rate of the exhaust gas, and the maximal temperature, three key "in-furnace" or internal quantities for establishing the MILD combustion. Importantly, however, changes of the initial separation of the fuel and air jets and the fuel injection angle are found to be most effective and efficient in controlling the flame performance and stability characteristics. These findings can be well-understood for the following reasons: First, different from conventional flame systems, commonly fitted with flame holders to avoid liftoff and blowout, the burners for MILD combustion must avoid any early molecular mixing between reactants, which enable the occurrence of combustion, or must "extinguish" visible flames near the injection exit. Second, the stable MILD combustion requires the local temperature to be above the point of autoignition and the local oxygen concentration to be sufficiently low, typically less than 10%. The mechanism to satisfy these conditions to control the oxidation process has to rely primarily upon the ways of delaying the effective molecular mixing process of fuel and oxygen through changing geometric and/or operational parameters. Also, it is found that the influence of all of the parameters studied, except for S and α, can be represented by the ratio of the fuel injection momentum to the air injection momentum, i.e., eq 3. However, with the present configuration of the recuperative furnace and burner system, the fuel penetration distance cannot be correctly estimated using the model of the strong jet/weak jet proposed by Grandmaison et al.,[26] perhaps because of the in-furnace flow structure being totally different from that proposed in the model. Note that the penetration distance can be well-obtained by the model in the forward flow configuration investigated by the present authors.[10]

AUTHOR INFORMATION

Corresponding Author
*E-mail: jcmi@coe.pku.edu.cn.

ACKNOWLEDGMENT

The first author gratefully acknowledges the support of the Nature Science Foundation of China (Grants 10921202 and 11072005). The present work is also funded by the Foundation of the State Key Laboratory of Coal Combustion of China.

REFERENCES

(1) Cavaliere, A.; de Joannon, M. *Prog. Energy Combust. Sci.* **2004**, *30*, 329–366.
(2) Tsuji, H.; Gupta, A. K.; Haskgawa, T.; Katsuki, M.; Kishimoto, K.; Morita, M. *High Temperature Air Combustion—From Energy Conservation to Pollution Reduction*; CRC Press (Taylor and Francis Group): Boca Raton, FL, 2003.
(3) Wünning, J. A.; Wünning, J. G. *Prog. Energy Combust. Sci.* **1997**, *23*, 81–94.
(4) Flamme, M. *Energy Convers. Manage.* **2001**, *42*, 1919–1935.
(5) Milani, A.; Saponaro, A. *IFRF Combust. J.* **2001**No. 200101.
(6) Katsuki, M.; Hasegawa, T. *Proc. Combust. Inst.* **1998**, *27*, 3135–3146.
(7) Weber, R.; Orsino, S.; Lallemant, N.; Verlaan, A. *Proc. Combust. Inst.* **2000**, *28*, 1315–1321.
(8) Weber, R.; Smart, J. P.; vd Kamp, W. *Proc. Combust. Inst.* **2005**, *30*, 2623–2629.
(9) Rottier, C.; Lacour, C.; Godard, G.; Taupin, B.; Porcheron, L.; Hauguel, R. *Proceedings of the European Combustion Meeting*; Vienna, Austria, 2009.
(10) Mi, J.; Li, P.; Zheng, C. *Energy* **2011**, DOI: 10.1016/j.energy.2011.09.003.
(11) Szegö, G.; Dally, B. B.; Nathan, G. J. *Combust. Flame* **2009**, *156*, 429–438.
(12) Szegö, G. Experimental and numerical investigation of a parallel jet mild combustion burner system in a laboratory-scale furnace. Ph.D. Thesis, The University of Adelaide, Adelaide, South Australia, Australia, 2010.
(13) Dally, B. B.; Riesmeier, E.; Peters, N. *Combust. Flame* **2004**, *137*, 418–431.

(14) Kumar, S.; Paul, P. J.; Mukunda, H. S. *Proc. Combust. Inst.* **2002**, *29*, 1131–1137.
(15) Mi, J.; Li, P.; Dally, B. B.; Craig, R. A. *Energy Fuels* **2009**, *23*, 5349–5356.
(16) Mi, J.; Li, P.; Zheng, C. *Chin. J. Chem. Eng.* **2010**, *18*, 10–17.
(17) Li, P.; Mi, J.; Dally, B. B.; Craig, R. A.; Wang, F. *Energy Fuels* **2011**, *25*, 2782–2793.
(18) Li, P.; Mi, J. *Flow, Turbul. Combust.* **2011**, *85*, 1–22.
(19) Schaffel-Mancini, N.; Mancini, M.; Szlek, A.; Weber, R. *Energy* **2010**, *35*, 2752–2760.
(20) Sobiesiak, A.; Rahbar, S.; Becker, H. A. *Combust. Flame* **1998**, *115*, 93–125.
(21) Weber, R.; Verlaan, A. L.; Orsino, S.; Lallemant, N. *J. Inst. Energy* **1999**, *72*, 77–83.
(22) ANSYS, Inc. *Fluent 6.3 Documentation*; ANSYS, Inc.: Canonsburg, PA, 2007.
(23) Pope, S. B. *Combust. Theory Modell.* **1997**, *1*, 41–63.
(24) Chui, E.; Raithby, G. *Numer. Heat Transfer, Part B* **1993**, *23*, 269–288.
(25) Mancini, M.; Weber, R.; Bollettini, U. *Proc. Combust. Inst.* **2002**, *29*, 1155–1162.
(26) Grandmaison, E. W.; Yimer, I.; Becker, H. A.; Sobiesiak, A. *Combust. Flame* **1998**, *114*, 381–396.
(27) Turns, S. *An Introduction to Combustion: Concepts and Applications*: McGraw-Hill: New York; 1996.
(28) Dally, B. B.; Shim, S. H.; Craig, R. A.; Ashman, P. J.; Szegö, G. *Energy Fuels* **2010**, *24*, 3462–3470.
(29) Dally, B. B.; Craig, R. A.; Mi, J. *Proceedings of the 9th Asia-Pacific International Symposium on Combustion and Energy Utilization*; Zhang, X., Liu, X., Eds.; World Publishing Corporation: Beijing, China, 2008; pp 35−40, ISBN: 978-7-5062-9284-9.